

Mechanism for enhancing dispersion of Co_3O_4 nanoparticles in Co/SiO_2 Fischer–Tropsch synthesis catalyst by adding glycol to impregnating solution: a quick-XAFS study

Naoto Koizumi,^{a,*} Shigenobu Suzuki,^a Yukiya Ibi,^a Yasuhiko Hayasaka,^a Yusuke Hamabe,^a Takayoshi Shindo^b and Muneyoshi Yamada^c

^aDepartment of Applied Chemistry, Graduate School of Engineering, Tohoku University, Aoba 6-6-07, Aramaki, Aoba-ku, Sendai 980-8579, Japan, ^bDepartment of Engineering in Applied Chemistry, Graduate School of Engineering and Resource Science, Akita University, 1-1 Tegatagakuen-machi, Akita 010-8502, Japan, and ^cAkita National College of Technology, 1-1 Iijima-Bunkyo-cho, Akita 011-8511, Japan. E-mail: nxk20@psu.edu

In situ Co *K*-edge quick-EXAFS (QEXAFS) coupled with temperature-programmed oxidation as well as *ex situ* XAFS was applied to investigating the mechanism for enhancing the dispersion of Co_3O_4 nanoparticles in a calcined Co/SiO_2 Fischer–Tropsch synthesis catalyst prepared by adding triethylene glycol (TEG) to a $\text{Co}(\text{NO}_3)_2 \cdot 6\text{H}_2\text{O}$ impregnating solution. *Ex situ* Co *K*-edge XAFS indicated that, regardless of whether the catalysts were prepared with or without using TEG, the hexaaqua Co (II) complex was formed in impregnated samples which then underwent the dehydration process to some extent during the subsequent drying step at 393 K. *In situ* QEXAFS and *ex situ* EXAFS results also indicated that small oxide clusters were formed in the TEG-modified catalyst calcined at ~ 400 – 470 K which interacted with polymer species derived from TEG. Since the Fischer–Tropsch synthesis activity of the TEG-modified catalyst increased with an increase in the calcination temperature in a similar temperature range [Koizumi *et al.* (2011), *Appl. Catal. A*, **395**, 138–145], it was suggested that such an interaction enables the clusters to be distributed over the support surface uniformly, resulting in enhancing their dispersion. After combustion of polymer species, Co_3O_4 -like species were formed, and agglomeration of the Co_3O_4 -like species at high calcination temperatures was suppressed by the addition of TEG to the impregnating solution. It was speculated that the addition of TEG induced the formation of some surface silicate which worked as an anchoring site for Co_3O_4 and Co^0 nanoparticles during calcination and H_2 reduction, respectively.

1. Introduction

Co-based catalysts are well known as typical Fischer–Tropsch synthesis (FTS) catalysts which synthesize mainly linear paraffins with a wide range of carbon numbers from CO and H_2 . These catalysts are usually prepared by impregnation of the aqueous solution containing $\text{Co}(\text{NO}_3)_2 \cdot 6\text{H}_2\text{O}$ into support materials such as Al_2O_3 , SiO_2 and TiO_2 followed by drying and calcination. Before the FTS, the calcined catalyst is reduced in H_2 to form FTS active Co^0 nanoparticles. Iglesia (1997)

reported that turnover frequencies of the supported catalysts were similar and almost independent of the size of the Co^0 particles when they were larger than 10 nm, which means that the rate of CO conversion normalized to the weight of Co increases with decreasing particle size in this range. Therefore, improvement of Co^0 dispersion without loss of reducibility of Co is an important strategy for enhancing the FTS activity.

Many efforts have been devoted so far to developing an effective preparation method for improving the dispersion of Co^0 . It was demonstrated that Co^0 nanoparticles with smaller sizes were formed after H_2 reduction when the catalyst was prepared using Co oxalate (Kraum & Baerns, 1999) and Co acetate (Sun *et al.*, 2000) as precursors instead of Co nitrate.

* Present address: Earth and Mineral Sciences Energy Institute, The Pennsylvania State University, C-211 Coal Utilization Laboratory, University Park, PA 16802, USA.

Unfortunately, however, use of these precursors produced significant amounts of Co silicate-like species which were hardly reduced to metallic state under normal conditions. Therefore most of the Co remained in an oxidized state even after H₂ reduction, and it suppressed the FTS activity of the catalysts greatly. In other words, trade-off relationships were reported between the dispersion of Co⁰ and the reducibility of Co in these studies. Several researchers pointed out the importance of a phenomenon occurring during impregnation in such precursor effects (Ming & Baker, 1995; Van Steen *et al.*, 1996; Trujillano *et al.*, 2007), although details of its origin have not been figured out yet.

In our recent studies it was revealed that the FTS activity of Co/SiO₂ was enhanced by adding a glycol such as ethylene glycol (EG), diethylene glycol and triethylene glycol (TEG) into the aqueous solution of Co(NO₃)₂·6H₂O (Koizumi *et al.*, 2011*a,b*). Interestingly, the addition of these glycols improved the dispersion of Co⁰ without loss of high reducibility of Co. *Ex situ* XRD and Co *K*-edge EXAFS analyses showed that Co₃O₄ nanoparticles with smaller size (~10 nm) were formed in the calcined catalyst without forming detectable quantities of Co silicate-like species when the catalyst was prepared using TEG. *Ex situ* Fourier-transform infrared spectroscopy (FT-IR) also provided evidence for the formation of the interaction between Co and TEG derivatives through Co–COO[−] bonds during calcination. Such an interaction could play a critical role in the formation of Co₃O₄ nanoparticles with high dispersion; however, it is still unclear yet how the glycols influence the formation process of precursor oxides to improve their dispersion.

Co *K*-edge XAFS is a powerful tool for investigating the speciation and coordination structures of Co formed during each preparation step for Co-based FTS catalysts because these Co species usually lack long-range order. In previous works, Co *K*-edge XAFS was mainly applied to the structural analysis of the calcined, reduced and used catalysts with regard to precursor effects (Khodakov *et al.*, 1997; Girardon *et al.*, 2007), support effects (Khodakov *et al.*, 2001; Morales *et al.*, 2004; Khodakov, 2009) and promoter effects (Morales *et al.*, 2004; Jacobs *et al.*, 2004*a*; Girardon *et al.*, 2007; Chu *et al.*, 2007). More recently, Jacobs and his colleagues (Jacobs *et al.*, 2007, 2010) successfully disclosed the reduction process of Co species in oxidized Co/SiO₂ and Co/Al₂O₃ under H₂ atmosphere by means of *in situ* quick-XAFS (QXAFS) coupled with temperature-programmed reduction, and reported how the reduction behaviour of Co was affected by the Co loading, type of support and the addition of the promoter. Furthermore, *ex situ* XAFS techniques provided useful insight into the deactivation mechanism of the Co-based FTS catalysts caused by, for example, co-product water (Jacobs *et al.*, 2002, 2003, 2004*b*; Das *et al.*, 2003).

On the other hand, use of Co *K*-edge (Q)XAFS was limited for investigating the speciation of Co and their coordination structures formed during each process of impregnation, drying and calcination. Girardon *et al.* (2007) reported XAFS spectra of impregnated and dried Ru/Re-promoted Co catalysts. In their experiments, some of their catalysts were prepared by

adding sucrose to the impregnating solutions. They demonstrated that the addition of sucrose to the impregnating solutions had minor influences on the Fourier-filtered $k^3\chi(k)$ of these catalysts, and suggested the importance of the subsequent calcination step in controlling the dispersion of Co⁰. In analogy to the studies by Jacobs *et al.* (2007, 2010), *in situ* Co *K*-edge QXAFS coupled with temperature-programmed oxidation (TPO) would be suitable for continuous monitoring of the changes in coordination structures caused by heating under oxidizing atmosphere, for example calcination, and provide useful information on the role of the organic additives. In spite of its potential usefulness, however, Co *K*-edge QXAFS of the Co-based catalysts during the calcination step have not been reported yet.

In this work, therefore, the coordination structures of Co formed in each process of catalyst preparation, namely impregnation, drying and calcination, and the effects of glycol addition to the impregnation solution on their coordination structures were investigated by *ex situ* and *in situ* Co *K*-edge XAFS to improve the understanding of the fundamental role of the glycols. Changes in the coordination structures of Co during the calcination step were continuously monitored by *in situ* QXAFS coupled with TPO, while *ex situ* XAFS was used for investigating the coordination structures of Co in the impregnated and dried catalysts. The mechanism for enhancing dispersion of the Co₃O₄ nanoparticles in the calcined catalyst is discussed based on these *ex situ* and *in situ* EXAFS data.

2. Experimental

2.1. Catalyst preparation

TEG-modified Co/SiO₂ catalysts were prepared by a pore-filling incipient wetness impregnation method. SiO₂ powder (BET surface area 224 m² g^{−1}, average pore diameter 15 nm, pore volume 1.24 ml g^{−1}, particle size 150–250 × 10^{−6} m) was calcined in static air at 823 K and 12 h before use, and impregnated with an aqueous solution containing Co(NO₃)₂·6H₂O (Wako Pure Chemical Industries, 99.5%) and TEG (Wako Pure Chemical Industries, 99.5%) followed by drying at 333 K for 2 h under flowing dry air (*i.e.* the first drying step). This sample was further dried at 393 K and 3 h (*i.e.* the second drying step) followed by calcination at 723 K for 4 h with a ramp rate of 1.0 K min^{−1}. Both these drying and calcination steps were carried out in static air. The Co loading of the catalyst was fixed at 20 mass% (SiO₂ weight basis). Since the FTS activity of the catalysts prepared using the impregnating solutions with different TEG–Co²⁺ molar ratios was maximized at ~0.25 mol mol^{−1} (Koizumi *et al.*, 2011*a,b*), the TEG–Co²⁺ molar ratios of 0.125 and 0.250 were chosen as typical values in this work. Hereafter, the catalysts thus prepared are designated as Co–TEG(*X*)/SiO₂, where *X* denotes the TEG-to-Co²⁺ molar ratio of the impregnating solution. Co/SiO₂ was also prepared using the aqueous solution containing only Co(NO₃)₂·6H₂O.

For investigating the coordination structures of Co in the impregnated sample, the sample which experienced impregnation followed by the first drying step was used for *ex situ* measurement because it was not easy to prepare a homogeneous wafer from the impregnated sample which contained large amounts of water. We confirmed that Co *K*-edge XAFS of impregnated Co/SiO₂ was similar to that of Co/SiO₂ dried at 333 K (not shown here). Besides, the ‘dried’ and ‘calcined’ catalysts (or samples) are defined as the catalysts which underwent the impregnation and (first and second) drying steps, and the impregnation (first and second) and drying steps followed by calcination, respectively.

2.2. XAFS measurements

Co *K*-edge XAFS of the catalysts were measured at BL14B2 at SPring-8 synchrotron radiation facility (Harima, Japan) with a ring energy of 8 GeV in quick-XAFS mode in transmission set-up. The X-rays passed through a Si(111) double-crystal monochromator and focused onto the sample. The EXAFS data were collected in transmission mode using *I*₀ and *I* ionization chambers filled with 100% N₂ and 15% Ar/N₂, respectively.

For *ex situ* measurements, the appropriate amount of the impregnated or dried samples was diluted tenfold with polyethylene glycol powder using a pestle and mortar, and then pressed into a self-supporting wafer (diameter 10 mm) at 25 MPa for 3 min. The amount of the sample was adjusted so that $\Delta \nu t$ of the sample fell within the range 0.7–1.0. XAFS measurements were carried out under ambient temperature with 100 s dwell time. On the other hand, *in situ* QXAFS coupled with TPO was used to monitor the change in the coordination structures of Co during calcination. The dried catalyst was mixed with the equivalent amount of boron nitride powder, and then pressed into a self-supporting wafer (diameter 10 mm) under medium pressure (12 MPa, 2 min). The thickness of this sample wafer was below 1 mm which is indispensable for reducing the diffusion resistance of gases into the wafer. The sample wafer was placed in an *in situ* XAFS cell made of quartz, and then the cell was connected to a flow system equipped with mass flow controllers. The sample was heated from 373 to 623 K at a ramp rate of 1 K min⁻¹ under flowing 20% O₂/He (99.99995%, ~100 ml min⁻¹). XAFS spectra were acquired every 180 s. Hereafter, the XAFS spectrum measured at *T* means that the spectrum was accumulated during $T \pm 1.5$ K. Tail gas from the *in situ* cell was analyzed simultaneously with an on-line mass spectrometer (MS) during *in situ* QXAFS experiments.

2.3. XAFS analysis

The observed Co *K*-edge XAFS were analyzed in a conventional manner including background subtraction and normalization followed by Fourier filtering using a Rigaku XAFS data analysis system (REX2000). Contributions from coordination shells in the Fourier-transformed $k^3\chi(k)$ were then inverse Fourier transformed with a Hanning-type window function into *k* space. Structural parameters of each coordi-

nation shell were determined by a non-linear least-squares fitting in *k* space. The backscattering amplitude and phase shift of Co–O and Co–Co coordination shells were extracted from Fourier-transformed $k^3\chi(k)$ of Co(NO₃)₂·6H₂O and Co foil, respectively. The number of independent parameters (*N*_{idp}) (Stern, 1993) was also calculated in accordance with the equation

$$N_{\text{idp}} = (2\Delta k \Delta R / \pi) + 2. \quad (1)$$

The quality of the fitting was evaluated by the *R*-factor (*R*_{*f*}) defined by the following equation,

$$R_f (\%) = \left\{ \frac{\sum_i [k^3 \chi_i^{\text{obs}}(k) - k^3 \chi_i^{\text{cal}}(k)]^2}{\sum_i [k^3 \chi_i^{\text{obs}}(k)]^2} \right\} \times 100. \quad (2)$$

Pattern-fitting analysis was also carried out for Co *K*-edge XANES of the catalysts to identify Co species in the catalysts. The *R*-factor defined by the following equation was used to evaluate the quality of the fitting,

$$R_f (\%) = \left[\frac{\sum (I_{\text{obs}} - I_{\text{cal}})^2}{\sum (I_{\text{obs}})^2} \right] \times 100. \quad (3)$$

3. Results and discussion

3.1. Coordination structures of Co in impregnated and dried samples

Impregnated (or dried) Co/SiO₂ and Co-TEG(0.25)/SiO₂ were used for *ex situ* Co *K*-edge XAFS. The effect of TEG on the coordination structures of Co formed in each preparation step was studied.

3.1.1. Co/SiO₂. Figs. 1(A) and 1(B) illustrate Co *K*-edge XANES and Fourier-transformed $k^3\chi(k)$ (FT-EXAFS) of impregnated Co/SiO₂, respectively. Since the aqueous solution of Co(NO₃)₂·6H₂O was used as the precursor, Co *K*-edge XANES and FT-EXAFS of Co(NO₃)₂·6H₂O are also included in these figures as references. In the nitrates of hexaaquacations such as Co(NO₃)₂·6H₂O and Ni(NO₃)₂·6H₂O, metal cations are surrounded by six oxygen atoms of H₂O ligands in octahedral structures (Bigoli *et al.*, 1971). Average Co–O bond distances are reported as 0.209 nm for both (NH₄)₂[Co(H₂O)₆](SO₄)₂ (Li & Li, 2004) and NH₄[Co(H₂O)₆]PO₄ (Bali *et al.*, 2005). As illustrated in Figs. 1(A) and 1(B), Co *K*-edge XANES of Co(NO₃)₂·6H₂O showed a characteristic white line at ~7720 eV, and an asymmetric peak ascribed to the Co–O coordination shell was observed in the FT-EXAFS at ~0.16 nm (phase shift not corrected). The Co–O bond distance determined by curve-fitting analysis was 0.208 nm which is in agreement with the literature value within the error of EXAFS analysis (± 0.002 nm; see Table 1).

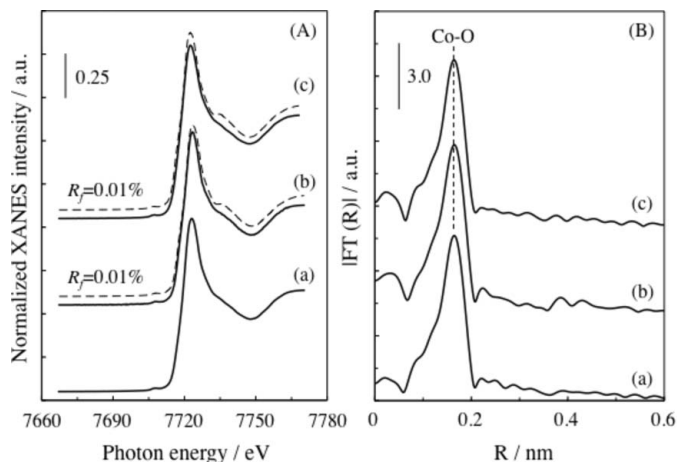
Co *K*-edge XANES and FT-EXAFS of impregnated Co/SiO₂ were similar to those of Co(NO₃)₂·6H₂O. Pattern-fitting analysis showed that the XANES spectrum of this sample was fitted with the reference spectrum as illustrated by a broken line in Fig. 1(A)–(b). Furthermore, the Co–O coordination

Table 1

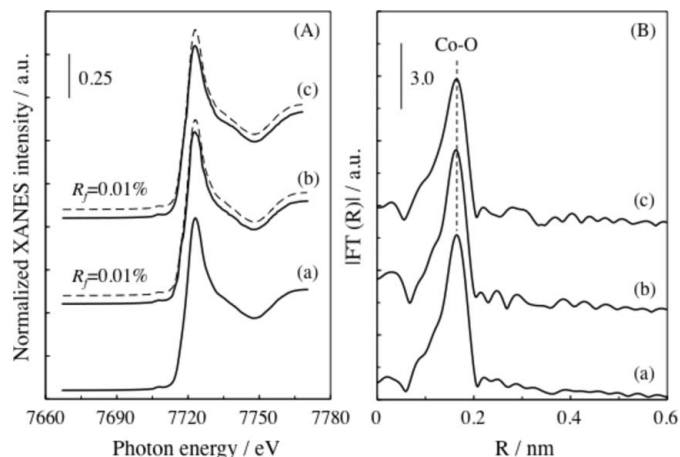
 Structural parameters of the Co–O coordination shell for Co/SiO₂ and Co-TEG(0.250)/SiO₂ after impregnation and drying steps.

 CN: coordination number; R : distance; E_0 : inner potential; σ^2 : Debye–Waller factor; N_{idp} : number of independent parameters defined by equation (1); R_f : R -factor; accuracy: CN ± 1.3 , $R \pm 0.002$ nm.

Sample		CN	R (nm)	E_0 (eV)	σ^2 (10^{-5} nm ²)	Δk (nm ⁻¹)	N_{idp}	R_f (%)
Co/SiO ₂	After impregnation	6.2	0.208	1.226	4.90	32.5–140	10	0.96
	After drying	5.2	0.207	−3.008	3.84	31.5–138	9	0.67
Co-TEG(0.250)/SiO ₂	After impregnation	5.8	0.208	0.289	4.36	32.5–141	10	1.04
	After drying	5.5	0.207	−2.246	5.18	32.0–141	10	0.62
Co(NO ₃) ₂ ·6H ₂ O	–	6.0 (fixed)	0.208	−0.733	4.76	32.5–143	10	0.66


Figure 1

Ex situ Co K -edge XANES (A) and FT-EXAFS (B) of Co(NO₃)₂·6H₂O (a), impregnated Co/SiO₂ (b) and impregnated Co-TEG(0.25)/SiO₂ (c). Pattern-fitting results for impregnated Co/SiO₂ and Co-TEG(0.25)/SiO₂ using the XANES of Co(NO₃)₂·6H₂O are illustrated by broken lines. The fitting quality (R_f) defined by equation (3) is also indicated in this figure. XAFS spectra were measured at ambient temperature.


Figure 2

Ex situ Co K -edge XANES (A) and FT-EXAFS (B) of Co(NO₃)₂·6H₂O (a), dried Co/SiO₂ (b) and dried Co-TEG(0.25)/SiO₂ (c). Pattern-fitting results for dried Co/SiO₂ and Co-TEG(0.25)/SiO₂ using the XANES of Co(NO₃)₂·6H₂O are illustrated by broken lines. The fitting quality (R_f) defined by equation (3) is also indicated in this figure. XAFS spectra were measured at ambient temperature.

number and bond distance calculated by fitting analysis were in agreement with those for reference Co(NO₃)₂·6H₂O (see Table 1). These results indicated that the hexaaqua Co (II) complex is the predominant Co species in the impregnated sample. Similarly, the Co K -edge XANES of dried Co/SiO₂ was fitted with the reference spectrum of Co(NO₃)₂·6H₂O [Fig. 2 (A)-(b)]. Although the Co–O coordination peak in the FT-EXAFS of the dried sample was less intense than that observed in the FT-EXAFS of Co(NO₃)₂·6H₂O as displayed in Fig. 2(B)-(b), curve-fitting analysis revealed that the difference in the Co–O coordination numbers for these samples was only 0.8, which was within the experimental error (± 1.3). Furthermore, no apparent difference was observed in the Co–O bond distances for the dried Co/SiO₂ and Co(NO₃)₂·6H₂O. In the thermal decomposition of Co(NO₃)₂·6H₂O, it is reported that the coordinated H₂O molecules were dehydrated to form anhydrous Co(NO₃)₂ at ~ 380 K via Co(NO₃)₂·4H₂O (~ 310 K) and Co(NO₃)₂·2H₂O (~ 340 K) (Ehrhardt *et al.*, 2005). In anhydrous Co(NO₃)₂, Co atoms are still surrounded by six oxygen atoms of NO₃ ligands, but the Co–O bond distance extends to ~ 0.211 nm (Grigori *et al.*, 2002). Taking the thermal decomposition experiments reported by Ehrhardt *et al.* (2005) into consideration, it is reasonable that dehydration of the hexaaqua Co (II) complex

indeed takes place during the drying step. Presumably, H₂O in ambient air would reabsorb during preparation of the sample wafer or the *ex situ* XAFS measurement which resulted in the formation of Co(NO₃)₂·6H₂O in the dried sample.

3.1.2. Co-TEG(0.25)/SiO₂. Co K -edge XANES and FT-EXAFS of impregnated Co-TEG(0.25)/SiO₂ are displayed in Figs. 1(A)-(c) and 1(B)-(c), and those of dried Co-TEG(0.25)/SiO₂ are depicted in Figs. 2(A)-(c) and 2(B)-(c), respectively. Both the XANES and FT-EXAFS of impregnated Co-TEG(0.25)/SiO₂ were similar to the reference spectra. As depicted by a broken line in Fig. 1(A)-(c), a comparable degree of fitting accuracy to impregnated Co/SiO₂ was obtained in pattern-fitting analysis for impregnated Co-TEG(0.25)/SiO₂ using the spectrum of Co(NO₃)₂·6H₂O. Furthermore, the $k^3\chi(k)$ and FT-EXAFS of impregnated Co-TEG(0.25)/SiO₂ were fitted with a single Co–O coordination shell as displayed in Figs. 3(a) and 3(b). The Co–O coordination number and bond distance calculated by curve-fitting analysis were similar to those for Co(NO₃)₂·6H₂O (see also Table 1). The Co K -edge XANES of dried Co-TEG(0.25)/SiO₂ was also fitted with the reference spectrum [Fig. 2(A)-(c)]. Curve-fitting analysis was then carried out on this sample using the Co–O coordination shell, and best-fitting results are displayed in Figs. 3(c) and 3(d). The Co–O bond distance and

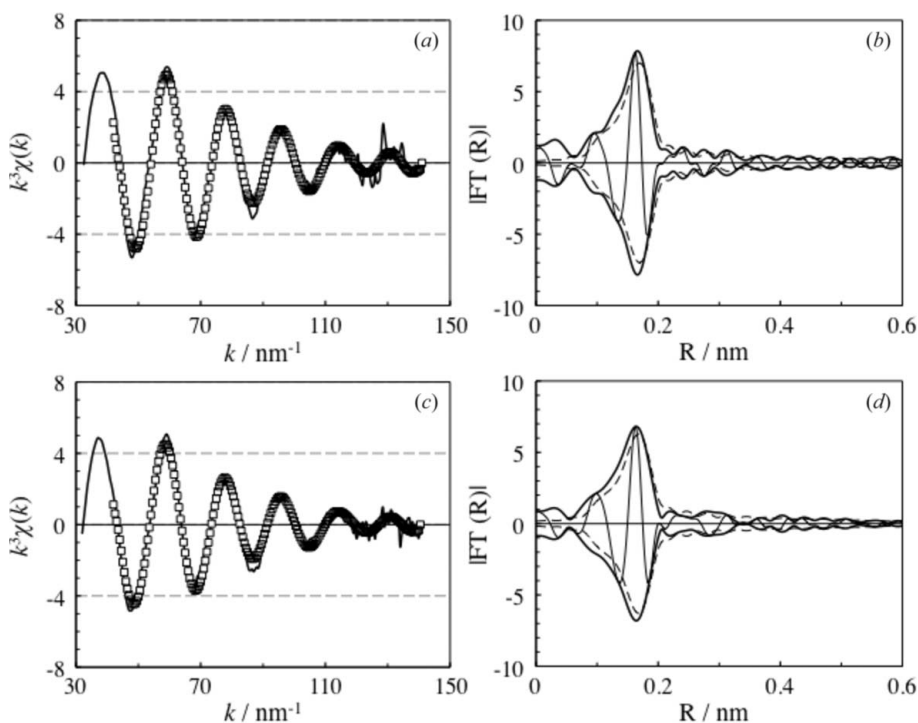


Figure 3 Best-fitting results for Co *K*-edge $k^3\chi(k)$ and FT-EXAFS of impregnated (*a, b*) and dried (*c, d*) Co-TEG(0.25)/SiO₂. Curve-fitting analysis was carried out using a single Co–O coordination shell. Fitting results are represented by open squares for $k^3\chi(k)$ and broken lines for FT-EXAFS.

coordination number were in agreement with those for Co(NO₃)₂·6H₂O within the experimental errors as tabulated in Table 1. These results suggested that the hexaaqua Co (II) complex is formed in impregnated Co-TEG(0.25)/SiO₂ which then undergoes the dehydration process to some extent during the subsequent drying step. The addition of TEG to the aqueous solution of Co(NO₃)₂·6H₂O caused no apparent differences in the coordination structures of Co in the impregnated and dried samples.

It is unlikely that H₂O ligands of the hexaaqua Co (II) complex are replaced with TEG because TEG itself is a weak ligand. On the other hand, it was reported that OH groups of TEG are oxidized at 318 K in the presence of nitric acid (Van Oijen *et al.*, 1994) to form a dicarboxylic acid. The dicarboxylic acid thus formed could be coordinated with Co through the formation of Co–COO bonds during the impregnation and drying steps like chelating agents such as nitrilotriacetic acid and *trans*-1,2-diaminocyclohexane-*N,N,N',N'*-tetraacetic acid (Mochizuki *et al.*, 2007). However, *ex situ* Co *K*-edge XAFS measurements in this work revealed that the addition of TEG to the impregnating solution had little influence on the coordination structures of Co formed in each preparation step. These results are of importance because several researchers have suggested that the

Co precursor effect is caused by interaction of Co with the organic additives which then affects the modes of interaction between Co and surface hydroxy groups during impregnation (Ming & Baker, 1995; Van Steen *et al.*, 1996; Trujillano *et al.*, 2007).

3.2. *In situ* monitoring of the coordination structure of Co during calcination

The change in coordination structures of Co during the calcination step, and how the addition of TEG to the impregnating solution affects them, were monitored by the *in situ* QEXAFS technique. The dried catalyst was mixed with BN powder, and placed in the *in situ* XAFS cell made of quartz. XAFS spectra were acquired every 180 s during heating of the catalyst under flowing 20% O₂/N₂. The tail gas was analyzed simultaneously with the on-line MS.

3.2.1. Co/SiO₂. Fig. 4 illustrates the change in the Co *K*-edge FT-EXAFS of

Co/SiO₂ measured during TPO. Two temperature regions were observed in terms of the change in the FT-EXAFS spectra. At low calcination temperatures (379–418 K), only a broad peak attributed to the Co–O coordination shell of Co(NO₃)₂·*n*H₂O (*n* < 6) was observed at ~0.16 nm (not phase-shift corrected). The intensity of this peak was reduced with increasing calcination temperature which was accompanied by a peak shift towards a shorter bond distance. The decrease in the peak intensity indicated that hydrating water was further eliminated from Co nitrate species. It would also result from increasing thermal disorder caused by heating. On the other hand, three peaks evolved at ~420 K followed by an increase in their

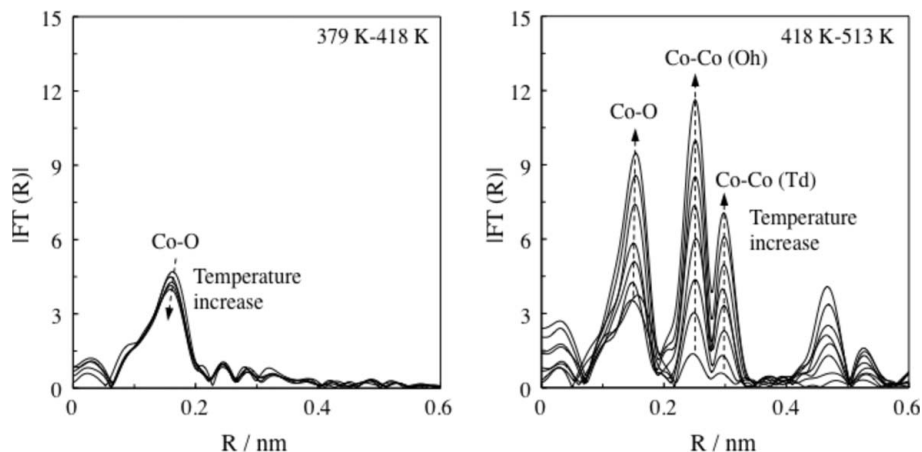
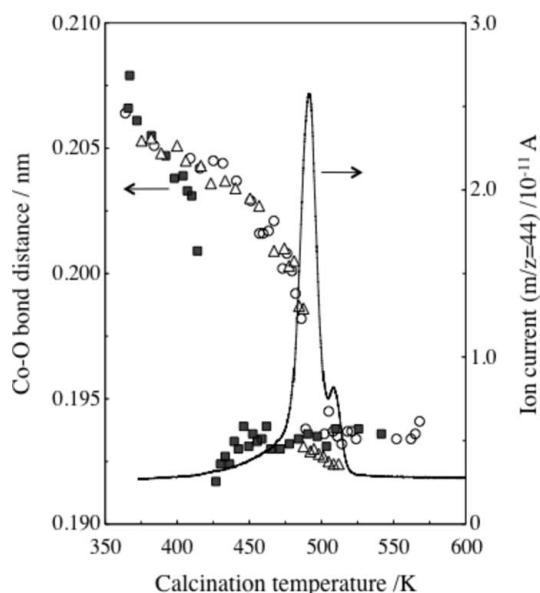


Figure 4 Co *K*-edge FT-EXAFS of dried Co/SiO₂ monitored by *in situ* QEXAFS coupled with TPO. The dried sample was heated under flowing 20% O₂/N₂ at a ramp rate of 1 K min⁻¹. XAFS spectra were acquired every 180 s during heating of the sample.


Figure 5

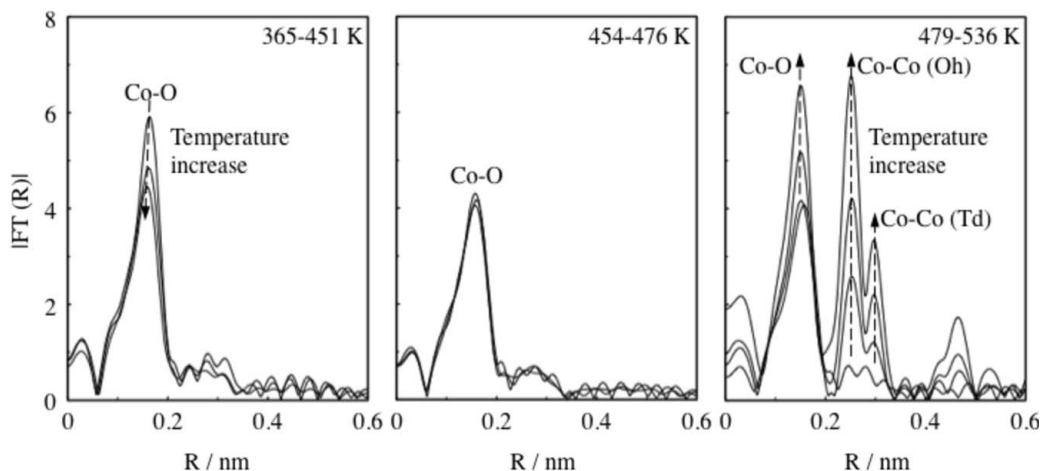
Change in the Co–O bond distances for Co/SiO₂ (closed squares), Co-TEG(0.125)/SiO₂ (open triangles) and Co-TEG(0.25)/SiO₂ (open circles) during heat treatment in a flow of 20% O₂/He. The Co–O bond distances were determined by curve-fitting analysis using Co *K*-edge FT-EXAFS illustrated in Figs. 4 and 6. This figure also illustrates the change in partial pressure of CO₂ monitored by on-line MS spectroscopy (*m/z* = 44) during the *in situ* experiment of Co-TEG(0.25)/SiO₂.

intensities with the calcination temperature. These three peaks are characteristic of Co₃O₄, and ascribed to the Co–O, Co–Co (Oh) and Co–Co (Td) coordination shells of Co₃O₄ (Koizumi *et al.*, 2009). The emergence of these peaks indicated that the Co nitrate species was decomposed to form Co₃O₄-like species. Increasing intensities of these peaks also indicated that Co₃O₄-like species were agglomerated at calcination temperatures higher than 420 K.

Since the difference in the Co–O bond distances for Co(NO₃)₂·6H₂O (0.207 nm) and Co₃O₄ (0.193 nm) is

approximately seven times larger than the typical error of EXAFS analysis (± 0.002 nm), the Co–O bond distance can be used as indexes for investigating in detail the decomposition of Co nitrate species into Co₃O₄-like species. The Co–O bond distances calculated by curve-fitting analysis are plotted in Fig. 5 as a function of the calcination temperature. It is seen from this figure that the Co–O bond distance decreased monotonically with an increase in calcination temperature from 360 to 410 K followed by an abrupt decrease at ~ 420 K. Above this temperature the bond distance slightly increased with calcination temperature, and was in agreement with that for polycrystalline Co₃O₄. This figure illustrates that the Co nitrate species is decomposed at ~ 415 K under the conditions used in this work. This decomposition temperature is lower than that reported for thermal decomposition of Co(NO₃)₂·6H₂O investigated by TG-DTA (~ 560 K) (Ehrhardt *et al.*, 2005).

3.2.2. Co-TEG(X)/SiO₂. Co *K*-edge FT-EXAFS of Co-TEG(0.25)/SiO₂ changed in a similar way to those observed for Co/SiO₂ as displayed in Fig. 6. However, the addition of TEG to the impregnating solution caused three major differences between their FT-EXAFS. First, an additional temperature region was observed for the TEG-modified catalyst in terms of change in the FT-EXAFS, namely 454–476 K. In this temperature range the FT-EXAFS spectra remained almost unchanged. The second one is related to the temperature for the formation of Co₃O₄-like species; Co₃O₄-like species were formed in Co-TEG(0.25)/SiO₂ at approximately 40 K higher temperatures than those in Co/SiO₂. Finally, the intensities of the peaks characteristic of Co₃O₄ for Co-TEG(0.25)/SiO₂ were no more than 50% of those observed for Co/SiO₂ at the higher calcination temperatures, indicating that agglomeration of Co₃O₄-like species was moderated by the addition of TEG. The latter is important because *in situ* QXAFS experiments provide direct evidence that the addition of TEG to the impregnating solution suppressed agglomeration of Co₃O₄-like species during calcination.


Figure 6

Co *K*-edge FT-EXAFS of dried Co-TEG(0.25)/SiO₂ monitored by *in situ* QXAFS coupled with TPO. The dried sample was heated under flowing 20% O₂/N₂ at a ramp rate of 1 K min⁻¹. XAFS spectra were acquired every 180 s during heating of the sample.

To investigate the effect of TEG in more detail, Co-TEG(0.125)/SiO₂ was also used for the *in situ* QXAFS experiment. The Co–O bond distances for Co-TEG(*X*)/SiO₂ (*X* = 0.125, 0.25) were then calculated by curve-fitting analysis, and are plotted in Fig. 5 as a function of the calcination temperature. When the calcination temperatures were lower than 400 K, the Co–O bond distances for Co-TEG(*X*)/SiO₂ decreased with an increase in the calcination temperature, similar to those for Co/SiO₂. However, a gradual decrease in the Co–O bond distances for the TEG-modified catalysts was observed between 400 and 470 K, resulting in deviation of the Co–O distances from those for Co/SiO₂. At higher calcination temperatures the Co–O bond distances for Co-TEG(*X*)/SiO₂ dropped to approximately 0.193 nm, indicating the formation of Co₃O₄-like species.

Fig. 5 also displays the change in partial pressure of CO₂ in the tail gas monitored by the on-line MS during the *in situ* QXAFS measurement of Co-TEG(0.25)/SiO₂. An intense peak of CO₂ (*m/z* = 44) was observed in the temperature range 473–523 K as displayed in this figure, whereas no CO₂ was observed during the *in situ* experiment of Co/SiO₂ (not shown here). Therefore, this intense peak is attributed to the combustion of carbonaceous species derived from TEG. It is seen from this figure that the formation of Co₃O₄-like species in Co-TEG(0.25)/SiO₂ was accompanied by the combustion of carbonaceous species. In other words, carbonaceous species derived from TEG were preserved in the catalyst before the formation of Co₃O₄-like species. Taking these results into consideration, it is reasonable that some kind of interaction is formed between Co and carbonaceous species in the range 400–470 K, which caused deviation of the Co–O bond distances for Co-TEG(*X*)/SiO₂ from those for Co/SiO₂. This is consistent with *ex situ* FT-IR results in our previous work where the IR band of the COO[−] ligand coordinated with Co was observed when the TEG-modified catalyst was calcined at 423 and 473 K (Koizumi *et al.*, 2011a).

3.3. Formation of small Co oxide clusters as a precursor for Co₃O₄-like species

Since *in situ* measurements at high temperatures would increase thermal disorder and may obscure EXAFS oscillation, the coordination structures of Co in Co-TEG(0.25)/SiO₂ calcined at different temperatures were further investigated by *ex situ* Co *K*-edge EXAFS for deeper understanding of the role of TEG. In this experiment the dried catalyst was calcined in an electric oven at a ramp rate of 1 K min^{−1}. Once the furnace temperature reached a desired calcination temperature, the catalyst was allowed to cool down to ambient temperature.

Fig. 7 illustrates Co *K*-edge FT-EXAFS of Co-TEG(0.25)/SiO₂ calcined at 423 and 473 K in comparison with that of dried Co-TEG(0.25)/SiO₂. Co oxalate [Co(C₂O₄)·2H₂O] was chosen as a reference Co compound which contains the Co–COO bonds, and used for the *ex situ* measurement as well. In the FT-EXAFS spectra of calcined Co-TEG(0.25)/SiO₂, asymmetric peaks were observed at ~0.16 nm (phase shift not

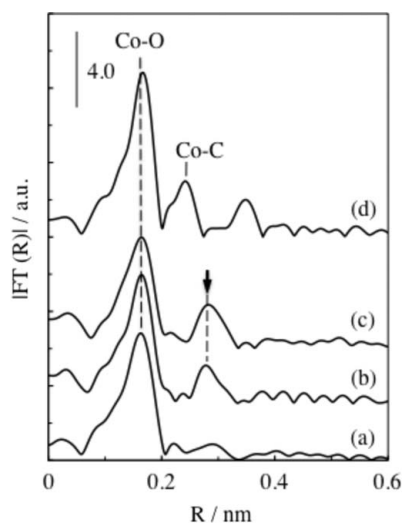


Figure 7

Ex situ Co *K*-edge FT-EXAFS of Co-TEG(0.25)/SiO₂ calcined at different temperatures in comparison with that of Co(C₂O₄)·2H₂O as a reference Co compound which has a Co–COO bond. XAFS spectra were measured at ambient temperature; dried Co-TEG(0.25)/SiO₂ (a), Co-TEG(0.25)/SiO₂ calcined at 423 K (b), Co-TEG(0.25)/SiO₂ calcined at 473 K (c) and Co(C₂O₄)·2H₂O (d).

corrected). The intensities of these peaks were weaker than that observed in the FT-EXAFS of the dried sample, which is consistent with the *in situ* QEXAFS results mentioned in §3.2.2. Besides these peaks, weak peaks were observed at ~0.27 nm (phase shift not corrected) in the FT-EXAFS of the calcined samples. They were never observed in the spectrum of the dried one, and did not match even with the Co–C coordination peak observed in the FT-EXAFS of Co oxalate. On the other hand, these new peaks are similar to the Co–Co coordination peaks of Co₃O₄-like species observed during the *in situ* QEXAFS experiments at high calcination temperatures. Then Co *K*-edge EXAFS of Co-TEG(0.25)/SiO₂ calcined at different temperatures were fitted with two coordination shells, namely Co–O and Co–Co coordination shells. Best-fitting results are displayed in Fig. 8. As can be seen from this figure, both the *k*³χ(*k*) and FT-EXAFS of Co-TEG(0.25)/SiO₂ were fitted well with these coordination shells. This indicates that Co nitrate species are decomposed to form Co oxide species in the TEG-modified catalysts calcined at 423–473 K. Optimized structural parameters for the C–O and Co–Co coordination shells are summarized in Table 2. The Co–Co distances were apparently longer than that for polycrystalline CoO (0.302 nm) (Khodakov *et al.*, 1997), but similar to that of the Co–Co (Td) coordination shell of polycrystalline Co₃O₄ (0.335 nm) (Khodakov *et al.*, 1997; Koizumi *et al.*, 2009). Conversely, the Co–Co coordination numbers for these catalysts were smaller than that of the Co–Co (Td) coordination shell of polycrystalline Co₃O₄ (2–3 versus 8). The small Co–Co coordination number for these samples suggested that small Co oxide clusters are formed during calcination in the range 400–473 K, although the accurate size of these oxide clusters is not clear because of relatively large errors in the Co–Co coordination numbers.

Table 2

Fitting results for Co *K*-edge $k^3\chi(k)$ spectra of Co(20)-TEG(0.25)/SiO₂ calcined at different temperatures (*T*).

CN: coordination number; *R*: distance; *E*₀: inner potential; σ^2 : Debye–Waller factor; *N*_{idp}: number of independent parameters defined by equation (1); *R*_f: *R*-factor; accuracy: CN(Co–O) ± 1.3, CN(Co–Co) ± 2.0, *R*(Co–O) ± 0.002 nm, *R*(Co–Co) ± 0.005 nm.

<i>T</i>	Scattering pair	CN	<i>R</i> (nm)	<i>E</i> ₀ (eV)	σ^2 (10 ^{−5} nm ²)	Δk (nm ^{−1})	<i>N</i> _{idp}	<i>R</i> _f (%)
423 K	Co–O	5.2	0.207	0.114	4.76	32.0–138	18	1.18
	Co–Co	1.6	0.316	−4.821	6.40			
473 K	Co–O	5.2	0.206	−1.574	6.08	33.0–140	18	0.70
	Co–Co	3.1	0.318	−3.100	9.80			

3.4. Role of TEG in enhancing dispersion of Co₃O₄ nanoparticles

Glycols such as EG are known as critical reagents for preparation of fine metal particles and uniform mixed oxides in the polyol process (Blin *et al.*, 1989) and polymerizable complex method (Kakihana *et al.*, 1993; Kakihana, 1996), respectively. In the polymerizable complex method, ester polymerization takes place between glycols and carboxylic acid such as citric acid. The polymer species thus formed consists of a three-dimensional carbon network, in which the metal complex is immobilized to form the polymer complex (Kakihana *et al.*, 1993; Kakihana, 1996).

In analogy to the polymerizable complex method, it is reasonable that TEG and dicarboxylic acid formed by the oxidation of TEG polymerize to form a three-dimensional carbon network before the formation of Co₃O₄-like species. In other words, the intense peak of CO₂ observed during the

in situ QEXAFS measurement of Co-TEG(0.25)/SiO₂ would be caused by the combustion of such a polymer species. Since the amount of TEG in Co-TEG(0.25)/SiO₂ was almost comparable with that required for monolayer coverage of the SiO₂ surface as reported previously (Koizumi *et al.*, 2011a), these polymer species can spread over the support surface uniformly. On the other hand, the *in situ* QEXAFS and *ex situ* EXAFS results described in §3.2 and §3.3 indicated that the small Co oxide clusters, hereafter simply denoted as Co_{*x*}O_{*y*}, were formed in Co-TEG(0.25)/SiO₂ calcined at ~400–473 K which interacted with these polymer species through coordination with their COO[−] ligands. In this regard it is highlighted that the FTS activity, CO conversion, of Co-TEG(0.25)/SiO₂ was dependent upon the calcination temperature, and increased with an increase of the calcination temperature in the range 423–523 K (Koizumi *et al.*, 2011a), which also indicated that dispersion of Co increased in this temperature range when the catalyst is prepared using TEG. Combining

these results, it is suggested that the Co_{*x*}O_{*y*}-polymer interaction during calcination enables the clusters to be distributed over the support surface, resulting in enhancing their dispersion during calcination. This explanation in turn suggests that such a dispersion enhancement effect does not work effectively at low TEG–Co²⁺ molar ratios owing to insufficient coverage of the support surface with polymer species. This could explain why there is an optimum TEG–Co²⁺ molar ratio for the FTS activity of the TEG-modified catalyst reported previously (Koizumi *et al.*, 2011a,b).

The formation of the Co_{*x*}O_{*y*}-polymer interaction indicated in this work also provides important insight into the optimum TEG–Co²⁺ molar ratio for Co-TEG(*X*)/SiO₂. In our previous work the FTS activity of the catalysts prepared using the impregnating solution with different TEG–Co²⁺ molar ratios was investigated at 503 K and 1.1 MPa using a fixed-bed reactor system, and maximized at ~0.25 (Koizumi *et al.*, 2011a,b). At this molar ratio the amount

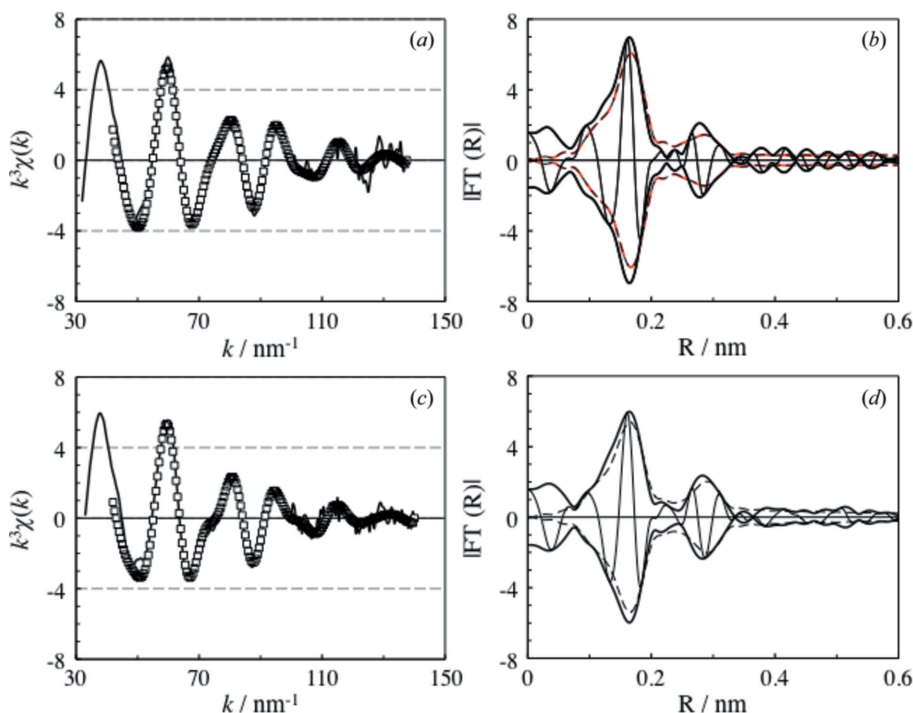


Figure 8

Best-fitting results for Co *K*-edge $k^3\chi(k)$ and FT-EXAFS of Co-TEG(0.25)/SiO₂ calcined at 423 K (*a*, *b*) and 473 K (*c*, *d*), indicating the formation of small oxide clusters in the calcined samples. Curve-fitting analysis was carried out using the Co–O and Co–Co coordination shells. Fitting results are represented by open squares for $k^3\chi(k)$ and broken lines for FT-EXAFS.

of Co was fourfold larger than that of TEG. This means that only part of the Co atoms can be involved in the complex formation, assuming the formation of the (1:1) complex, even if all the OH groups of TEG are oxidized to COOH groups. This is in marked contrast with the fact that an excess amount of carboxylic acid is used in the polymerizable complex method. Since the carbon number of TEG is 6, the carbon–cobalt atomic ratio is 1.5 at the optimum TEG–Co²⁺ molar ratio. Under such a low atomic ratio it is difficult to immobilize Co atoms in a three-dimensional carbon network as suggested for the polymerizable complex method. On the other hand, the *ex situ* Co *K*-edge EXAFS measurements of calcined Co-TEG(0.25)/SiO₂ indicated that small precursor oxide clusters were preserved in the carbon network before the formation of Co₃O₄-like species. Assuming that these precursor oxides have a structure similar to the minimum structure fragment of Co₃O₄, namely the unit cell (see Fig. 9), the Co–Co (Td) and Co–Co (Oh) coordination numbers are calculated to be 3.1 and 3.3, respectively. These coordination numbers are similar to those observed experimentally for calcined Co-TEG(0.25)/SiO₂ as mentioned in §3.3. Since this model structure consists of 34 Co atoms, the carbon–Co_xO_y molar ratio is about 50 at the optimum TEG–Co²⁺ molar ratio which enables uniform distribution of Co_xO_y in the carbon network.

The QEXAFS experiments in this work also revealed that Co₃O₄-like species were formed after combustion of polymer species, and that agglomeration of these oxide species was retarded by the addition of TEG to the impregnating solution. Since polymer species are already removed from the catalyst surface by combustion in this calcination temperature range, a different mechanism should be involved in the retarded agglomeration of Co₃O₄-like species. In this regard it is worth noting that the formation of surface silicate is facilitated by the use of an organic Co precursor (Girardon *et al.*, 2005) and/or addition of organic ligands (Trujillano *et al.*, 2007, 2008). It is also noted that our QEXAFS results do not rule out the formation of such silicate-like species other than Co_xO_y and Co₃O₄-like species. Therefore, it is speculated that the addition of TEG induced the formation of some surface silicate species which would work as anchoring sites for Co₃O₄ and Co⁰ species during calcination and H₂ reduction, respectively

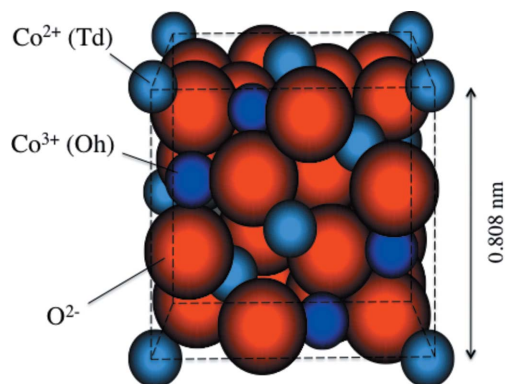


Figure 9
Structural model for small oxide clusters observed in Co-TEG(0.25)/SiO₂ calcined at 423 and 473 K. This structural model is created based on the Co₃O₄ unit cell structure, and consists of 34 Co atoms.

(Lim *et al.*, 2007). In other words, TEG has two different functions of controlling speciation and coordination environments of Co, leading to the formation of Co₃O₄ species with high dispersion in the calcined catalyst.

4. Conclusion

In situ Co *K*-edge QXAFS coupled with TPO as well as *ex situ* XAFS was applied to investigating coordination structures of Co formed in each preparation step of Co/SiO₂ and Co-TEG/SiO₂ for understanding the mechanism for enhancing dispersion of Co₃O₄ nanoparticles caused by the addition of TEG to the impregnating solution. The change in coordination structures of Co during calcination was continuously monitored by *in situ* QEXAFS coupled with TPO, while *ex situ* XAFS was used for investigating coordination structures of Co in the impregnated and dried catalysts. The following are the important results obtained in this work.

(i) The coordination structure of Co formed in impregnated Co/SiO₂ was similar to that of the hexaaqua Co (II) complex which then underwent the dehydration process to some extent during the subsequent drying step at 393 K. The addition of TEG to this impregnating solution caused no apparent differences in these coordination structures.

(ii) During calcination, the Co nitrate species in Co/SiO₂ was dehydrated, and then decomposed to form Co₃O₄-like species at about 415 K followed by their agglomeration at high temperatures.

(iii) *In situ* QEXAFS and *ex situ* EXAFS results indicated that small oxide clusters were formed in the TEG-modified catalyst calcined at ~400–470 K which interacted with polymer species derived from TEG. Taking our previous result into consideration, it was suggested that such an interaction enables the clusters to be distributed over the support surface uniformly, resulting in an enhancement of their dispersion during calcination.

(iv) *In situ* QEXAFS results also revealed that Co₃O₄-like species were formed after combustion of polymer species, and that agglomeration of the Co₃O₄-like species at high temperatures was suppressed by the addition of TEG to the impregnating solution. It was speculated that the addition of TEG induced the formation of some surface silicate species which worked as anchoring sites for Co₃O₄ and Co⁰ species during calcination and H₂ reduction, respectively.

This research was supported by the Japan Society for the Promotion of Science (JSPS), Grant-in-Aid for Scientific Research (S), 17106011, 2005. EXAFS measurement was performed at BL14B2 at SPring-8 with the approval of JASRI (proposal No. 2009B1835). We gratefully thank the staff of SPring-8 for their technical support and their kind help.

References

- Bigoli, F., Braibanti, A., Tiripicchio, A. & Camellini, M. T. (1971). *Acta Cryst.* **B27**, 1427–1434.
Blin, B., Fievet, F., Beaupere, D. & Figlarz, M. (1989). *Nouv. J. Chim.* **13**, 67–72.

- Chu, W., Chernavskii, P. A., Gengembre, L., Pankina, G. A., Fongarland, P. & Khodakov, A. Y. (2007). *J. Catal.* **252**, 215–230.
- Das, T. K., Jacobs, G., Patterson, P. M., Conner, W. A., Li, J. & Davis, B. H. (2003). *Fuel*, **82**, 805–815.
- Ehrhardt, C., Gjikaj, M. & Brockner, W. (2005). *Thermochem. Acta*, **432**, 36–40.
- El Bali, B., Essehli, R., Capitelli, F. & Lachkar, M. (2005). *Acta Cryst. E* **61**, i52–i54.
- Girardon, J.-S., Lermotov, A. S., Gengembre, L., Chernavskii, P. A., Griboval-Constant, A. & Khodakov, A. Y. (2005). *J. Catal.* **230**, 339–352.
- Girardon, J.-S., Quinet, E., Griboval-Constant, A., Chernavskii, P. A., Gengembre, L. & Khodakov, A. Y. (2007). *J. Catal.* **248**, 143–157.
- Grigorii, A. T., Konstantin, O. Z., Igor, V. M., Erhard, K. & Sergei, L. T. (2002). *Z. Anorg. Allg. Chem.* **628**, 269–273.
- Iglesia, E. (1997). *Appl. Catal. A*, **161**, 59–78.
- Jacobs, G., Chaney, J. A., Patterson, P. M., Das, T. K. & Davis, B. H. (2004a). *Appl. Catal. A*, **264**, 203–212.
- Jacobs, G., Das, T. K., Patterson, P. M., Li, J., Sanchez, L. & Davis, B. H. (2003). *Appl. Catal. A*, **247**, 335–343.
- Jacobs, G., Ji, Y., Davis, B. H., Cronauer, D., Kropf, A. J. & Marshall, C. L. (2007). *Appl. Catal. A*, **333**, 177–191.
- Jacobs, G., Ma, W., Davis, B. H., Cronauer, D., Kropf, A. J. & Marshall, C. L. (2010). *Catal. Lett.* **140**, 106–115.
- Jacobs, G., Patterson, P. M., Das, T. K., Luo, M. & Davis, B. H. (2004b). *Appl. Catal. A*, **270**, 65–76.
- Jacobs, G., Patterson, P. M., Zhang, Y., Das, T. K., Li, J. & Davis, B. H. (2002). *Appl. Catal. A*, **233**, 215–226.
- Kakihana, M. (1996). *J. Sol-Gel Sci. Technol.* **6**, 7–55.
- Kakihana, M., Yashima, M., Yoshimura, M., Mazaki, H. & Yasuoka, H. (1993). *J. Jpn. Soc. Powder Powder Metall.* **40**, 137–145.
- Khodakov, A. Y. (2009). *Catal. Today*, **144**, 251–257.
- Khodakov, A. Y., Griboval-Constant, A., Bechara, R. & Villain, F. (2001). *J. Phys. Chem. B*, **105**, 9805–9811.
- Khodakov, A. Y., Lynch, J., Bazin, D., Rebours, B., Zanier, N., Moisson, B. & Chaumette, P. (1997). *J. Catal.* **168**, 16–25.
- Koizumi, N., Mochizuki, T. & Yamada, M. (2009). *e-J. Surf. Sci. Nanotechnol.* **7**, 633–640.
- Koizumi, N., Suzuki, S., Niiyama, S., Ibi, Y., Shindo, T. & Yamada, M. (2011a). *Appl. Catal. A*, **395**, 138–145.
- Koizumi, N., Suzuki, S., Niiyama, S., Shindo, T. & Yamada, M. (2011b). *Catal. Lett.* **141**, 931–938.
- Kraum, M. & Baerns, M. (1999). *Appl. Catal. A*, **186**, 189–200.
- Li, X.-H. & Li, Z.-G. (2004). *Acta Cryst. E* **60**, i114–i115.
- Lim, S., Wang, C., Yang, Y., Ciuparu, D., Pfefferle, L. & Haller, G. L. (2007). *Catal. Today*, **123**, 122–132.
- Ming, H. & Baker, B. G. (1995). *Appl. Catal. A*, **123**, 23–36.
- Mochizuki, T., Koizumi, N., Hamabe, Y., Hara, T. & Yamada, M. (2007). *J. Jpn. Petrol. Inst.* **50**, 262–271.
- Morales, F., De Groot, F. M. F., Glatzel, P., Kleimenov, E., Bluhm, H., Halvecker, M., Knop-Gericke, A. & Weckhuysen, B. M. (2004). *J. Phys. Chem. B*, **108**, 16201–16207.
- Stern, E. A. (1993). *Phys. Rev. B*, **48**, 9825–9827.
- Sun, S., Tsubaki, N. & Fujimoto, K. (2000). *Appl. Catal. A*, **202**, 121–131.
- Trujillano, R., Lambert, J.-F. & Louis, C. (2008). *J. Phys. Chem. C*, **112**, 18551–18558.
- Trujillano, R., Villain, F., Louis, C. & Lambert, J.-F. (2007). *J. Phys. Chem. C*, **111**, 7152–7164.
- Van Oijen, A. H., Huck, N. P. M., Kruijtzter, J. A. W., Erkelens, C., Van Boom, J. H. & Liskamp, R. M. J. (1994). *J. Org. Chem.* **59**, 2399–2408.
- Van Steen, E., Sewell, G. S., Makhothe, R. A., Micklethwaite, C., Manstein, H., De Lange, M. & O’Conner, C. T. (1996). *J. Catal.* **162**, 220–229.